ISSN (Print) 1226-1750
ISSN (Online) 2233-6656
Journal of Magnetics 22(4), 630-636 (2017) https://doi.org/10.4283/JMAG.2017.22.4.630

Separation and Calculation of Photoneutron and Photoproton in 10MV and 15MV LINACs

Jeong-Ho Kim[1] and Seok-Hwan Bae[2]*

[1]*Department of Radiation Oncology, Konyang University Hospital, Daejeon 35365, Republic of Korea*
[2]*Department of Radiological Science, College of Medical Science, , Konyang University, Daejeon 35365, Republic of Korea*

(Received 23 August 2017, Received in final form 18 October 2017, Accepted 18 October 2017)

The photoneutron ray and photoproton ray occur according to the use of the high-energy electromagnetic radiation of LINACs. Here, when measuring the photoneutron ray, the measurement of the photoproton ray is added due to the characteristics of the measurement instruments for neutrons, so the reliability of the measurement value is low. Therefore, in this study, the self-manufactured solenoid was used to measure the photoneutron and photoproton rays, and the calculation formula using a reaction cross-section was applied to verify reliability. For the 10 MV LINACs and 15 MV LINACs, the proper conditions of the solenoid were evaluated for their application, and for distances of 80 cm, 100 cm and 120 cm from the source to the measurement instrument, the photoneutron dose value and the sum value of the photoneutron dose and photoproton dose values were read according to the installation of the solenoid in the radiation field of 5 × 5 cm^2, 10 × 10 cm^2 and 15 × 15 cm^2. In addition, the calculation formula according to the reaction cross-section was applied to derive a nuclear reaction process number for the test conditions, and a ratio of the photoneutron ray value on the photoproton ray value was compared. The comparison results showed that reliability within 10 % was verified, and in the further measurement of the photoneutron ray and photoproton ray on the LINACs, the usefulness of the solenoid was verified.

Keywords : photoneutron, photoproton, solenoid, medical LINAC

1. Introduction

As the use of high-energy electromagnetic radiation is generalized from the development of LINACs (Linear Accelerators), interest on the occurrence of photoneutron on the LINACs are increasing [1]. Accordingly, measurements are attempted across various methods to evaluate this photoneutron. The computation using the Monte Carlo Simulation is quoted as the most general approach method [2-7]. However, this Monte Carlo Simulation is a result of calculation by computerizing the proof and formula in existing studies, so the measurement results cannot always be correct [8-10]. Moreover, in the actual measurements, there are cases of the actual measurement value being lower in reliability due to the overlap caused by various errors. Also, the measurement instrument used in the measurement of the photoneutron uses a general measurement instrument for neutrons, and this instrument cannot separate from its baryonic radiation due to the measurement principle [11-13]. From the photonuclear reaction with the substance, the high-energy electromagnetic radiation of the LINACs releases not only neutrons, but also various other types of radiation such as scattered photons, electrons and protons [6, 14, 15]. Therefore, when using the measurement instrument for neutrons when measuring the photoneutron, the measurement of photoproton was added together. In other words, the measurement of the photoneutron in existing tests must consider the dosage of photoproton [16-18]. So, for the separation method of the photoneutron and photoproton, the electric charge was considered to realize the magnetic field for separation. For the realization of the magnetic field, a solenoid was used, and the dosage calculation of the photoneutron and photoproton was possible by separating the photoproton. Therefore, in this study, the photoneutron and photoproton were separated and calculated in the 10MV and 15MV LINACs.

*Corresponding author: Tel: +82-42-600-8439
Fax: +82-42-600-9468, e-mail: shbae@konyang.ac.kr

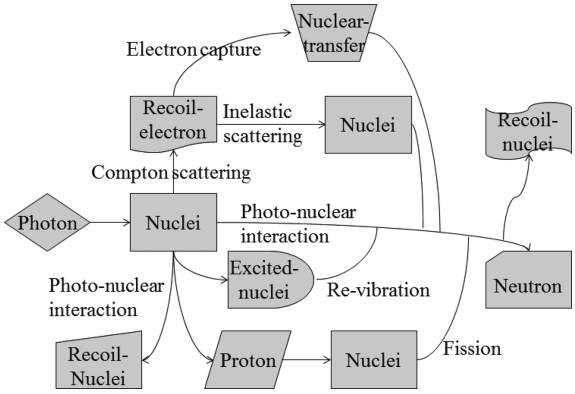

Fig. 1. Mechanism of production photoneutron.

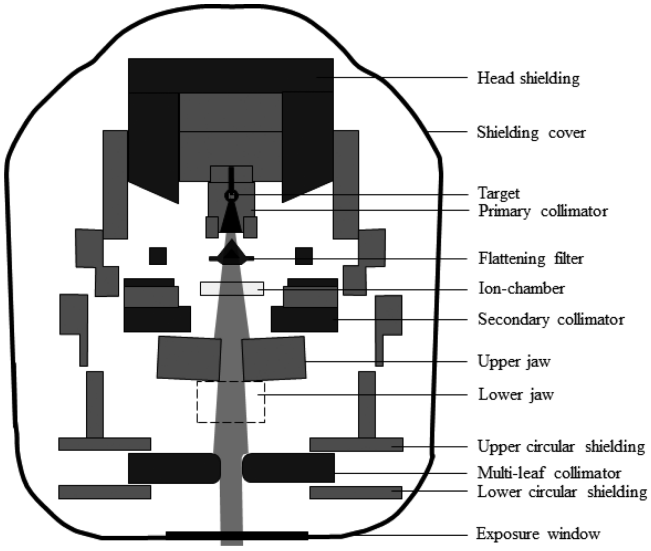

Fig. 2. Structure of LINAC head.

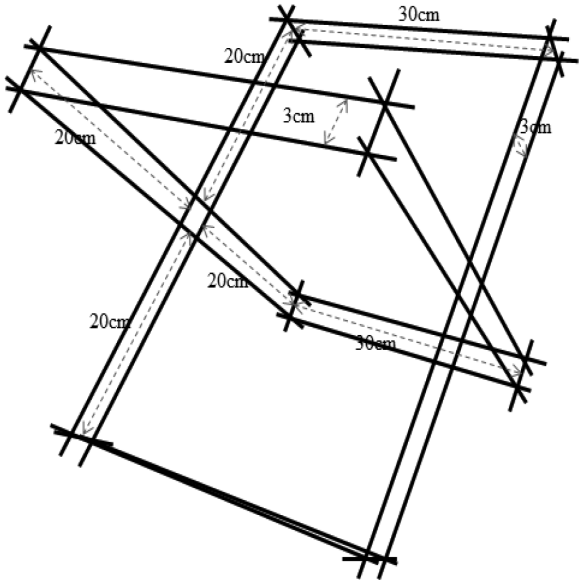

Fig. 3. Structure of solenoid.

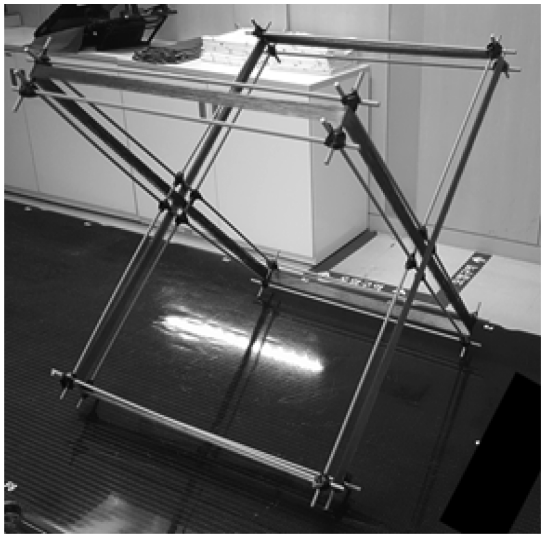

Fig. 4. Image of solenoid.

2. Materials and Methods

2.1. Equipment and materials

1. Medial LINACs : CLINAC-iX (VARIAN, USA) 10 MV machine, 15 MV machine
2. Neutron detector : Optically Stimulated Luminescence Neutron (LANDAUER, USA)
3. Handmade Solenoid
4. Cubic Phantom : Solid Phantom (CIRS, USA) 30 cm × 30 cm × 20 cm
5. Electron detector : LINACHECK (PTW, GERMANY)

2.2. Experimental

2.2.1. Production of handmade solenoid

The solenoid was manufactured for excluding the photoproton by the magnetic field. However, the magnetic field is formed on the vertical direction on the direction of the solenoid coil winding [19, 20]. Therefore, to maintain the direction of the magnetic field in the horizontal direction, the solenoid coil and frame were maintained within the beam to influence the beam. Thus, the direction of the magnetic field was maintained in the horizontal direction, but to prevent the structure from being positioned inside the beam, the solenoid in the structure shown in Fig. 4 was manufactured. The magnetic field is formed in left direction due to the coils winded to the right of the frame, and vice versa. Here, when the current is applied in the same direction, the magnetic field is formed in the horizontal direction by the vector sum of the magnetic field in both the left and right directions to satisfy the condition. However, as the structure of the

Table 1. Spec of Solenoid.

Number of Coil around	208 cm^{-1}
Input Voltage	12 V
Inner Diameter	30 cm to 43 cm

solenoid becomes enlarged according to the radiation field, it was manufactured as shown in Fig. 3, and the measurement is enabled only in the radiation field condition of within 20 × 20 cm^2.

For the specification of the solenoid, the coil was winded 208 times per unit length, the applied voltage is 12 V, and the inside diameter measures 30 cm-43 cm. Here, the magnetic field strength (B) depends on the applied current (I) and the number of coils winded per unit length (n) as shown in Formula 1, so the angle of diffraction according to the applied current must be measured.

$$B_{tot} = \sqrt{(k \times n_{ro} \times i_{ro})^2 + (k \times n_{lo} \times i_{lo})^2} \quad (1)$$

B_{tot} : Intensity of magnetic field in transverse axis [T]
k : Constant [N/A^2]
n_{ro} : Number of coiling at a unit length in right-oblique axis [m^{-1}]
n_{lo} : Number of coiling at a unit length in left-oblique axis [m^{-1}]
i_{ro} : Intensity of input current in right-oblique axis [A]
i_{lo} : Intensity of input current in left-oblique axis [A]

2.2.2. Measurement of slop angle and intensity of magnet field for current

To calculate the angle of diffraction on the photoproton according to the use of a solenoid, it is impossible through the direct measurement. Therefore, the angle of diffraction on the electron beam is measured, and then the angle of diffraction calculates the indirection through the momentum ratio of the electron beam and the proton beam. As shown in Fig. 6, the measurement method of the angle of diffraction on the electron beam is used to apply the current when the solenoid is mounted to read the measurement value according to the position of the radiation measurement instrument of the LINACHECK. Here, the conditions of the electron beam are shown in Table 2.

Also, the momentum of the electron beam and the proton beam by the 10 MV and 15 MV electromagnetic radiations is shown in Table 3.

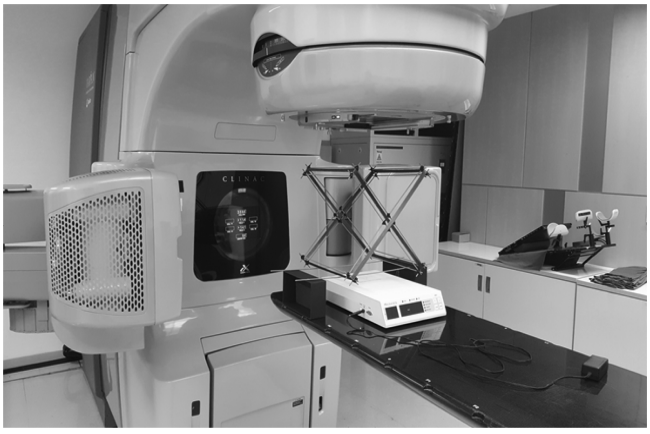

Fig. 5. Set up solenoid.

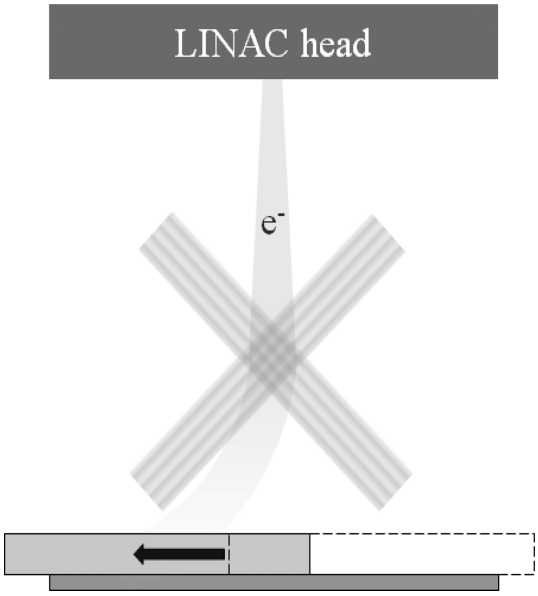

Fig. 6. Measurement of electron.

Table 2. Condition of electron beam.

Energy	18 MeV
SDD (Source to Detector Distance)	100 cm
Field size	10 × 10 cm^2
Electron Cone	Not use

Table 3. Quantity of motion from photoneutron and photoproton.

Class	Electron	Proton	
		10 MV	15 MV
Energy[a]	1.8×10^7 eV	1.65×10^5 eV	3.57×10^5 eV
Weight[b]	9.1×10^{-28} g	1.7×10^{-24} g	1.7×10^{-24} g
Speed[c]	1.99×10^{17} m/s	4.41×10^{14} m/s	6.48×10^{14} m/s
Quantity of Motion[d]	1.81×10^{-10} g·m/s	7.49×10^{-10} g·m/s	1.10×10^{-9} g·m/s

2.2.3. Calculation of cross-section

The calculation formula using the reaction cross-section as in Formula 2 was applied to compare the occurrence numbers of the photoneutron beam and the photoproton beam from the high-energy electromagnetic radiation of LINACs.

$$N = 6.022 \times 10^{23} \times \delta \times \nu \times \omega \quad (2)$$

N : Number of atoms
δ : Density
ν : Volume of materials
ω : Atomic weight

The information on the parts positioned inside the beam of the LINACs Gantry head is shown in Table 4. As for

Table 4. Information of part of LINAC head.

Accessory	Volume[a]	Materials	Atomic weight[b]	Density[c]	Number of atom
Flattening filter	$\frac{5}{3}\times 800\pi$	^{208}Pb	207.2	11.34	$\frac{6.022\times 11.34}{207.2}\times 10^{23}\times\frac{5}{3}\times 800\pi$
Ion chamber	$3\times\left(\frac{40\times 15.75}{100}\right)^2$	^{28}Si	28.0855	2.3290	$\frac{6.022\times 119.1}{28.0855}\times 10^{23}\times 3\times\left(\frac{40\times 15.75}{100}\right)^2$
Upper jaw	$9.5\times\left\{\left(\frac{40\times 26.25}{100}\right)^2-\left(\frac{A\times 26.25}{100}\right)^2\right\}$	^{184}W	183.84	19.25	$\frac{6.022\times 19.25}{183.84}\times 10^{23}\times 9.5\times\left\{\left(\frac{40\times 26.25}{100}\right)^2-\left(\frac{A\times 26.25}{100}\right)^2\right\}$
Lower jaw	$9.5\times\left\{\left(\frac{40\times 33}{100}\right)^2-\left(\frac{A\times 33}{100}\right)^2\right\}$				$\frac{6.022\times 19.25}{183.84}\times 10^{23}\times 9.5\times\left\{\left(\frac{40\times 33}{100}\right)^2-\left(\frac{A\times 33}{100}\right)^2\right\}$
MLC	$9.5\times\left[\left\{\left(\frac{A\times 46.5}{100}\right)^2-\left(\frac{A\times 46.5}{2\times 100}\right)^2\times\pi\right\}\right]$	^{184}W	183.84	19.25	$\frac{6.022\times 19.25}{183.84}\times 10^{23}\times 9.5\times\left\{\left(\frac{A\times 46.5}{100}\right)^2-\left(\frac{A\times 46.5}{2\times 100}\right)^2\times\pi\right\}$
Exposure window	$0.5\times\left(\frac{A}{2}\times\frac{55.5}{100}\right)^2\times\pi$	^{12}C	12.0000	2.267	$\frac{6.022\times 2.267}{12}\times 10^{23}\times 0.5\times\left(\frac{A}{2}\times\frac{55.5}{100}\right)^2\times\pi$
		^{2}H	1.00794	0.8988	$\frac{6.022\times 0.8988}{1.00794}\times 10^{23}\times 0.5\times\left(\frac{A}{2}\times\frac{55.5}{100}\right)^2\times\pi$
Phantom	$20\times\left(\frac{A}{2}\times\frac{D}{100}\right)^2\times\pi$	^{12}C	12.0000	2.267	$\frac{6.022\times 2.267}{12}\times 10^{23}\times 20\times\left(\frac{A}{2}\times\frac{D}{100}\right)^2\times\pi$
		^{2}H	1.00794	0.8988	$\frac{6.022\times 0.8988}{1.00794}\times 10^{23}\times 0.5\times\left(\frac{A}{2}\times\frac{D}{100}\right)^2\times\pi$
		^{16}O	15.9994	1.429	$\frac{6.022\times 1.429}{15.9994}\times 10^{23}\times 20\times\left(\frac{A}{2}\times\frac{D}{100}\right)^2\times\pi$

A: Field Length [cm], *L*: Distance [cm], *K*: Number of photons per 1 MU [MU-1], *I*: Input MU[MU]
[a]Ref. [cm^3], [b]Ref. [g/mol], [c]Ref. [g/cm^3]

Table 5. Number of exposure photon.

Accessory	Number of photons	Accessory	Number of photons
Flattening filter	$K\times I\times\frac{5}{3}\times 800\pi$	Multileaf collimator	$K\times I\times 9.5\times\left[\left\{\left(\frac{A\times 46.5}{100}\right)^2-\left(\frac{A\times 46.5}{2\times 100}\right)^2\times\pi\right\}\right]$
Ion chamber	$K\times I\times 3\times\left(\frac{40\times 15.75}{100}\right)^2$	Exposure window	$K\times I\times 0.5\times\frac{A}{2}-\left(\frac{55.5}{100}\right)^2\times\pi$
Upper jaw	$K\times I\times 9.5\times\left\{\left(\frac{40\times 26.25}{100}\right)^2-\left(\frac{A\times 26.25}{100}\right)^2\right\}$	Phantom	$K\times I\times 20\times\left(\frac{A}{2}\times\frac{D}{100}\right)^2\times\pi$
Lower jaw	$K\times I\times 9.5\times\left\{\left(\frac{40\times 33}{100}\right)^2-\left(\frac{A\times 33}{100}\right)^2\right\}$		

Table 6. Cross-section of photoneutron and photoproton.

Accessory	Materials	Photoneutron			Photoproton		
		Cross-section[a]		Threshold Energy[b]	Cross-section[a]		Threshold Energy[b]
		10MV	15MV		10MV	15MV	
Flattening filter	^{208}Pb	100	450	7.37	10	35	8.01
Ion chamber	^{28}Si	0	0	17.18	0	0.2	11.58
Jaw	^{184}W	75	380	7.41	8.1	41.3	7.7
MLC	^{184}W	75	380	7.41	8.1	41.3	7.7
Exposure window	^{12}C	0	0	18.72	0	0	15.96
	^{2}H	1.43	0.96	2.22	-	-	-
Phantom	^{12}C	0	0	18.72	0	0	15.96
	^{2}H	1.43	0.96	2.22	-	-	-
	^{16}O	0	0	15.66	0	0.1	12.13

[a]Ref. [mb], [b]Ref. [MeV]

the incident photon number, the incident photon number inside the beam cannot be calculated, so a random constant number of a K value is applied. In other words, the instrument unit of the LINACs applying the equal dosage in the STP (Standard Temperature and Pressure, 0 °C 1 atm) condition is applied, and K value of incident photon number is judged to be shown per 1 MU, expressed as in Table 5. The reaction cross-section for each part is shown in Table 6 accordingly [21, 22].

2.2.4. Measurement of OSLN

As shown in Fig. 7, to measure the dose value of the photoneutron and photoproton with the solenoid mounted, the radiation field is classified as 5 × 5 cm^2, 10 × 10 cm^2 and 15 × 15 cm^2 for SDD 80 cm, 100 cm and 120 cm, and 10 MV and 15 MV electromagnetic radiations are irradiated as shown in Table 7. In the equal condition, the irradiation is performed without a solenoid mounted. The measurement is performed 10 times each to read and compare the neutron dosage.

Table 7. Condition of photon beam.

Energy	10 MV, 15 MV
SDD	80 cm, 100 cm, 120 cm
Field size	5 × 5 cm^2, 10 × 10 cm^2, 15 × 15 cm^2
Dose	500 MU
Doserate	600 MU/min
Gantry angle	0°
Collimator angle	0°

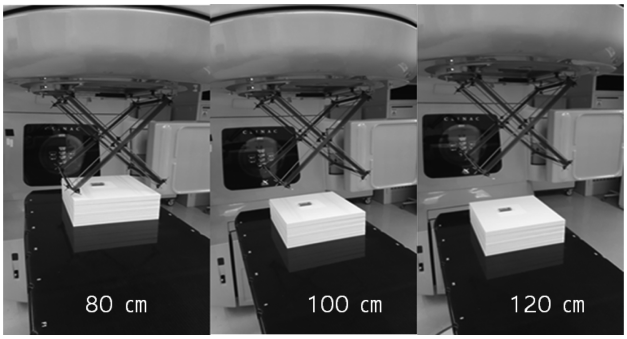

Fig. 7. Measurement of OSLN.

3. Result

3.1. Diffraction of solenoid from each current

The results according to the applied current of the power supply are shown in Fig. 8, and the angle of

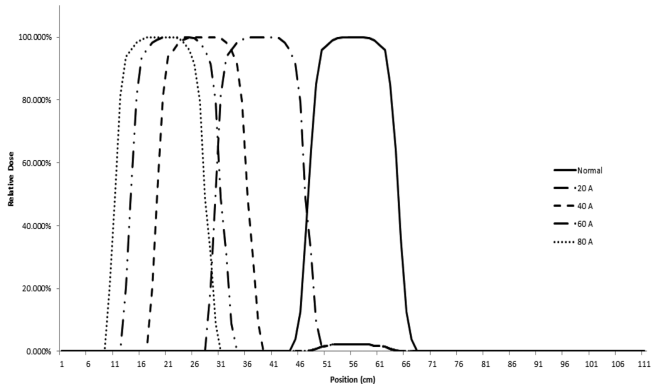

Fig. 8. Stray range from each current.

Table 8. Slop angle and intensity of magnetic field from each current.

Current	Stray range	Slop angle	magnetic field
20 A	10.5 cm	36.59°	0.37 T
40 A	21.5 cm	56.66°	0.74 T
60 A	33.5 cm	67.11°	1.11 T
80 A	46.5 cm	73.08°	1.48 T

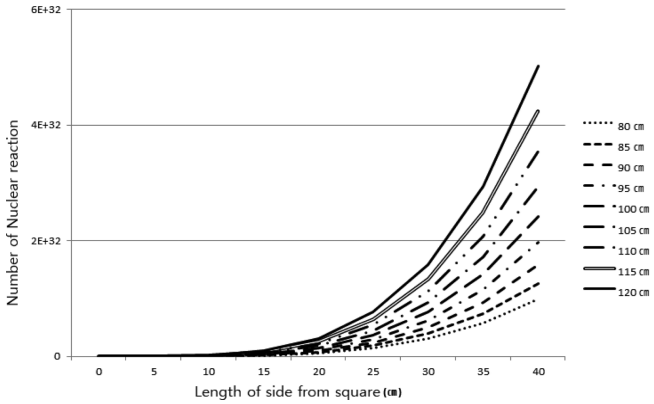

Fig. 9. Number of photoneutron interaction from 10 MV photon.

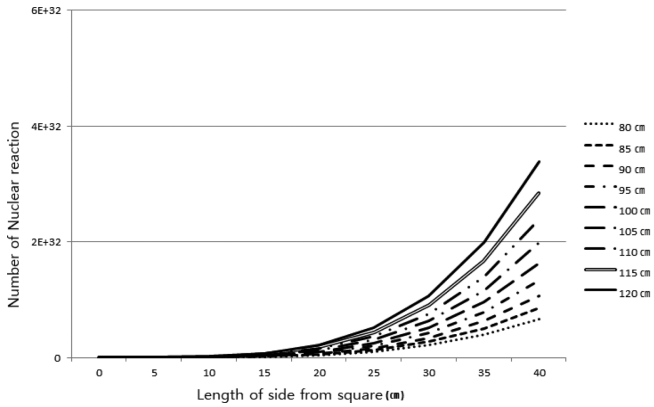

Fig. 10. Number of photoneutron interaction from 15 MV photon.

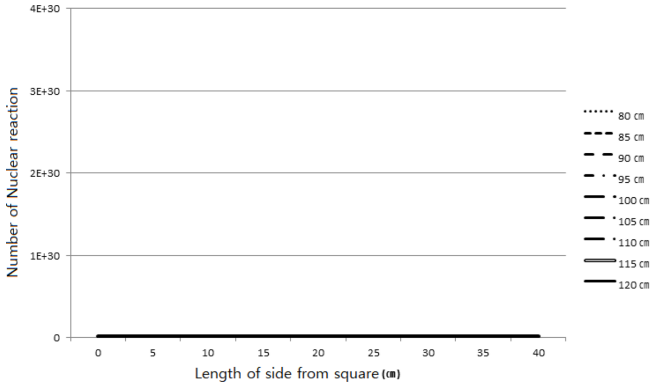

Fig. 11. Number of photoproton interaction from 10 MV photon.

diffraction according to the applied current, moving distance, and the magnetic field strength are shown in Table 8.

3.2. Number of photoneutron and photoproton reaction by calculation

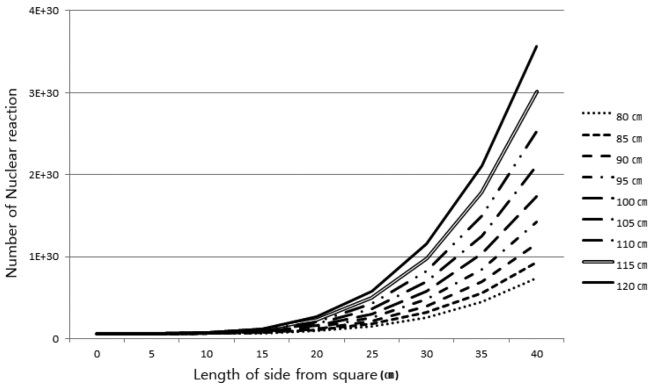

Fig. 12. Number of photoproton interaction from 15 MV photon.

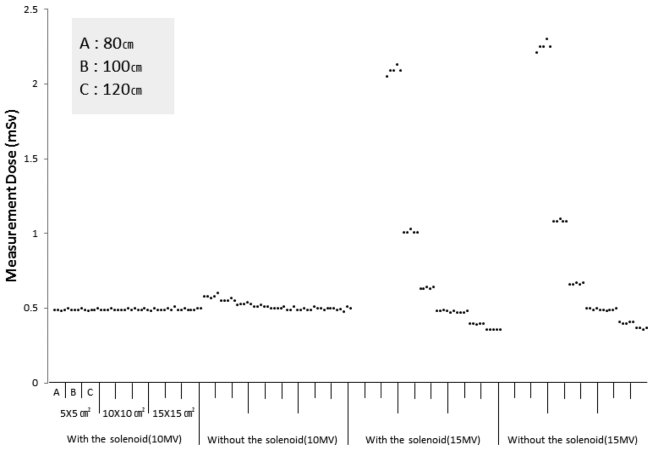

Fig. 13. Result of OSLN.

The reaction number of photoneutron and photoproton on the 10 MV and 15 MV electromagnetic radiations according to the measurement is shown in Fig. 9 to Fig. 12 according to the radiation field and distance.

3.3. Dose of photoneutron and photoproton using OSLN

The results of dosage measurement using OSLN are shown in Fig. 13.

4. Discussion

The comparison results of the ratio values of the photoneutron beam and photoproton beam derived from the measured and calculated values are shown in Fig. 14 to Fig. 15. The difference between calculated values and the measured values is within 10 % to be considered relatively reliable, but the condition of radiation field and distance is very small, so in the future, the conditions should be segmentalized and diversified to perform a

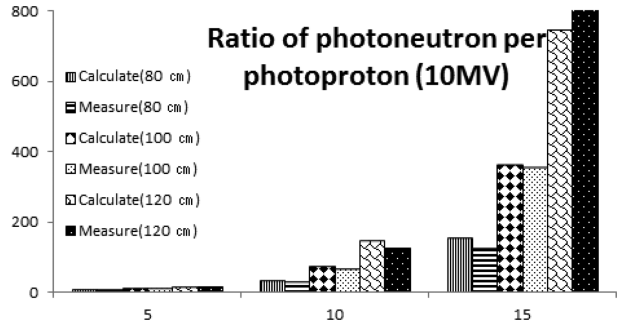

Fig. 14. Ratio of photoneutron per photoproton at 10MV.

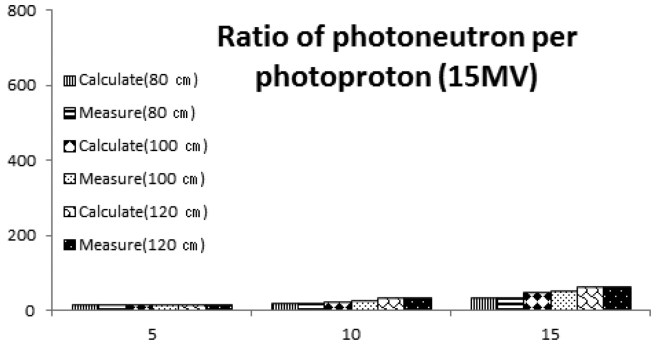

Fig. 15. Ratio of photoneutron per photoproton at 15MV.

separation and calculation on the photoproton and photoneutron.

5. Conclusion

As with the use of the high-energy electromagnetic radiation of LINACs becomes more commonplace, the photoneutron and photoproton beams would occur through interaction. Here, the measurement instrument for neutrons is used to measure the photoneutron beams, but due to the characteristics of the measurement instrument, the measurement value of the photoproton is included to have an error. Therefore, a self-manufactured solenoid was used to separate and measure the photoneutron beam and the photoproton beam for verifying the reliability of the measurement value, and a calculation formula was used to derive the nuclear reaction process number. Except for the photoproton beam occurred in the 10MV electromagnetic radiation, the dose value was increased as the radiation field was increased, and the range of increase was also enhanced as the distance increased. In addition, the dose measurement value of the photoproton beam can be derived depending on the installation of the solenoid, and similar results were shown to the calculation formula results using the actual reaction cross-section. Therefore, by measuring the photoproton dose value that was not possible in the existing LINACs, and measuring the photoneutron dose value that lacked reliability, the propriety of the exclusion method using the solenoid was verified.

References

[1] M. T. Kim, H. K. Lee, Y. C. Heo, and J. H. Cho, J. Magn. **19**, 15 (2014).
[2] Y. Laosiritaworn and W. Laosiritaworn, J. Magn. **20**, 11 (2015).
[3] S. Zabihinpoor and M. Hasheminia, Advanced Studies in Theoretical Physics **5**, 421 (2011).
[4] M. Tatari and A. H. Ranjbar, Ann. Nucl. Energy **63**, 69 (2014).
[5] C. Ongaro, A. Zanini, U. Nastasi, J. Ródenas, G. Ottaviano, and C. Manfredotti, Phys. Med. Biol. **45**, 55 (2000).
[6] F. d'Errico, R. Nath, L. Tana, G. Curzio, and W. G. Alberts, Med. Phys. **25**, 1717 (1998).
[7] H. Ghiasi and A. Mesbahi, Iranian J. Radiat. Res. **8**, 187 (2010).
[8] G. Atkinson and A. M. Nevill, Sports Medicine **26**, 217 (1998).
[9] A. Zanini, E. Durisi, F. Fasolo, L. Visca, C. Ongaro, U. Nastasi, and J. R. M. Annand, Radiat. Prot. Dosimetry **110**, 157 (2004).
[10] M. Kralik, K. Turek, and V. Vondráček, Radiat. Prot. Dosimetry **132**, 13 (2008).
[11] J. D. Irish, A. Buchnea, and D. B. McConnell, Nuclear Instruments and Methods in Physics Research **96**, 125 (1971).
[12] A. Veyssière, H. Beil, R. Bergère, P. Carlos, J. Fagot, A. Leprêtre, and J. Ahrens, Nucl. Instrum. Methods Phys. Res. **165**, 417 (1979).
[13] J. E. E. Baglin and M. N. Thompson, Nucl. Instrum. Methods in Phys. Res. **71**, 71 (1969).
[14] S. R. M. Mahdavi, Radiation Oncology **92**, 236 (2009).
[15] C. Ongaro, U. Nastasi, and A. Zanini, Monte Carlo Methods and Applications **5**, 69 (1999).
[16] E. V. Weinstock and J. Halpern, Physical Review **94**, 1651 (1954).
[17] K. Shoda, Phys. Rep. **53**, 341 (1979).
[18] V. G. Shevchenko and B. A. Yuryev, Nuclear Physics **37**, 495 (1962).
[19] V. Kumar, Am. J. Phys. **77**, 737 (2009).
[20] J. E. Kunzler, Rev. Mod. Phys. **33**, 501 (1961).
[21] R. Montalbetti, L. Katz, and J. Goldemberg, Phys. Rev. **91**, 659 (1953).
[22] L. Katz and A. G. W. Cameron, Can. J. Phys. **29**, 518 (1951).